nature geoscience

LETTERS

PUBLISHED ONLINE: 10 AUGUST 2015 | DOI: 10.1038/NGEO2493

Rapid increases in tropospheric ozone production and export from China

Willem W. Verstraeten[1,2]*, Jessica L. Neu[3], Jason E. Williams[2], Kevin W. Bowman[3], John R. Worden[3] and K. Folkert Boersma[1,2]

Rapid population growth and industrialization have driven substantial increases in Asian ozone precursor emissions over the past decade[1], with highly uncertain impacts on regional and global tropospheric ozone levels. According to ozonesonde measurements[2,3], tropospheric ozone concentrations at two Asian sites have increased by 1 to 3% per year since 2000, an increase thought to contribute to positive trends in the ozone levels observed at North America's West Coast[4,5]. However, model estimates of the Asian contribution to North American ozone levels are not well-constrained by observations[6,7]. Here we interpret Aura satellite measurements of tropospheric concentrations of ozone and its precursor NO_2, along with its largest natural source, stratospheric ozone, using the TM5 global chemistry–transport model. We show that tropospheric ozone concentrations over China have increased by about 7% between 2005 and 2010 in response to two factors: a rise in Chinese emissions by about 21% and increased downward transport of stratospheric ozone. Furthermore, we find that transport from China of ozone and its precursors has offset about 43% of the 0.42 DU reduction in free-tropospheric ozone over the western United States that was expected between 2005 and 2010 as a result of emissions reductions associated with federal, state and local air quality policies. We conclude that global efforts may be required to address regional air quality and climate change.

Elevated tropospheric ozone (O_3) concentrations have a direct adverse impact on human[8] and ecosystem health[9] at the surface, whereas in the free troposphere O_3 acts as a greenhouse gas[8,10] and drives the production of the hydroxyl radical, which controls the chemical lifetime of many atmospheric pollutants and reactive greenhouse gases. Previous studies have pointed not only to changing emissions of O_3 precursors[6,7,11–14], but also to changes in both the net inflow of O_3 from the stratosphere[14–16] and large-scale transport patterns[7,13–16] as contributing to observed trends and variability in tropospheric O_3. For many regions outside Asia, *in situ* measurements suggest that tropospheric O_3 has remained relatively constant in the 2000s following substantial increases in the 1980s–1990s, at least partially due to changes in the emissions of O_3 precursors, including nitrogen oxides (NO_X) and hydrocarbons[17]. However, chemistry–transport models used for attribution of trends in Europe and North America tend to greatly underestimate the observed O_3 changes over the past several decades[18]. Furthermore, trends are generally derived from sparse surface and balloon measurements that are not necessarily representative of larger regions. This is particularly true for China, where measurements from only two ozonesonde stations are reported in the literature[2,3].

Over the past decade, satellite instruments have provided valuable information on the global distribution of tropospheric O_3 and NO_X concentrations and their evolution in time. Here we use O_3 retrievals from the Tropospheric Emission Spectrometer (TES) and Microwave Limb Sounder (MLS) sensors and NO_2 from the Ozone Monitoring Instrument (OMI), all onboard NASA's Aura satellite (Methods). We investigate changes in TES tropospheric O_3 and OMI NO_2 over China and the western United States (US) between 2005 and 2010, and attribute the observed O_3 changes to emissions, transport and chemistry using the TM5 chemistry–transport model[19] (Methods), with both emissions and stratosphere–troposphere exchange constrained by the satellite measurements.

During summertime, when photochemical tropospheric O_3 production is most active, TES observes substantial increases of >10 DU in the partial O_3 column (3–9 km) over eastern China between 2005–2006 and 2009–2010 (Fig. 1a–c). At the same time, OMI observes NO_2 column increases of $>1.5\times10^{15}$ molecules cm^{-2} (Fig. 1d–f). Figure 1a–c also reveals a strong increase in O_3 off the coast of China (>6.0 DU), suggestive of O_3 production and transport aloft via the dominant westerlies[12], and weaker increases over the eastern Pacific ($\sim$3.7 DU). OMI observes significant reductions in NO_2 ($>0.3\times10^{15}$ molecules cm^{-2}) over much of the western US, especially California and Washington (Fig. 1d–f). TES shows decreases in O_3 over the western US in the areas with the largest NO_2 decreases, but the region as a whole shows an O_3 increase of $\sim$2.7 DU.

Monthly averaged O_3 values derived from TES measurements show the detailed temporal evolution of partial O_3 columns (3–9 km) for eastern China and the western US (Fig. 2a,e). These results are not strongly dependent on sampling (Supplementary Information 1). We interpret the observed satellite O_3 short-term trends with simulations from TM5 (Fig. 2a,e). To account for the rapid changes in NO_X emissions that have occurred between 2005 and 2010 (as reflected in OMI NO_2 measurements in Fig. 1), we use monthly means of the OMI tropospheric NO_2 column record to derive improved estimates of global monthly NO_X emissions for 2005–2010 (Methods and Supplementary Information 2). These top-down estimates[20], in line with published trends (Methods), indicate a 21% increase in NO_X over China from 25.1 to 30.3 Tg yr^{-1} NO_X for 2005–2010 (Supplementary Table 1). Over the western US, a 21% decrease is estimated (4.8 to 3.8 Tg yr^{-1} NO_X) following strict American emission controls for vehicles and power plants[21].

In our attribution of the observed signals in tropospheric O_3, we consider the effects of changes in anthropogenic NO_X emissions, stratosphere–troposphere exchange of ozone (STE) and long-range transport. We focus on NO_X emissions rather than other

[1]Wageningen University, Meteorology and Air Quality Group, Wageningen, Droevendaalsesteeg 4, 6708 PB Wageningen, The Netherlands. [2]Royal Netherlands Meteorological Institute, Satellite Observations, PO Box 201, NL-3730 AE De Bilt, The Netherlands. [3]Jet Propulsion Laboratory, California Institute of Technology, 4800 Oak Grove Drive, Pasadena, California 91109, USA. *e-mail: willem.verstraeten@wur.nl

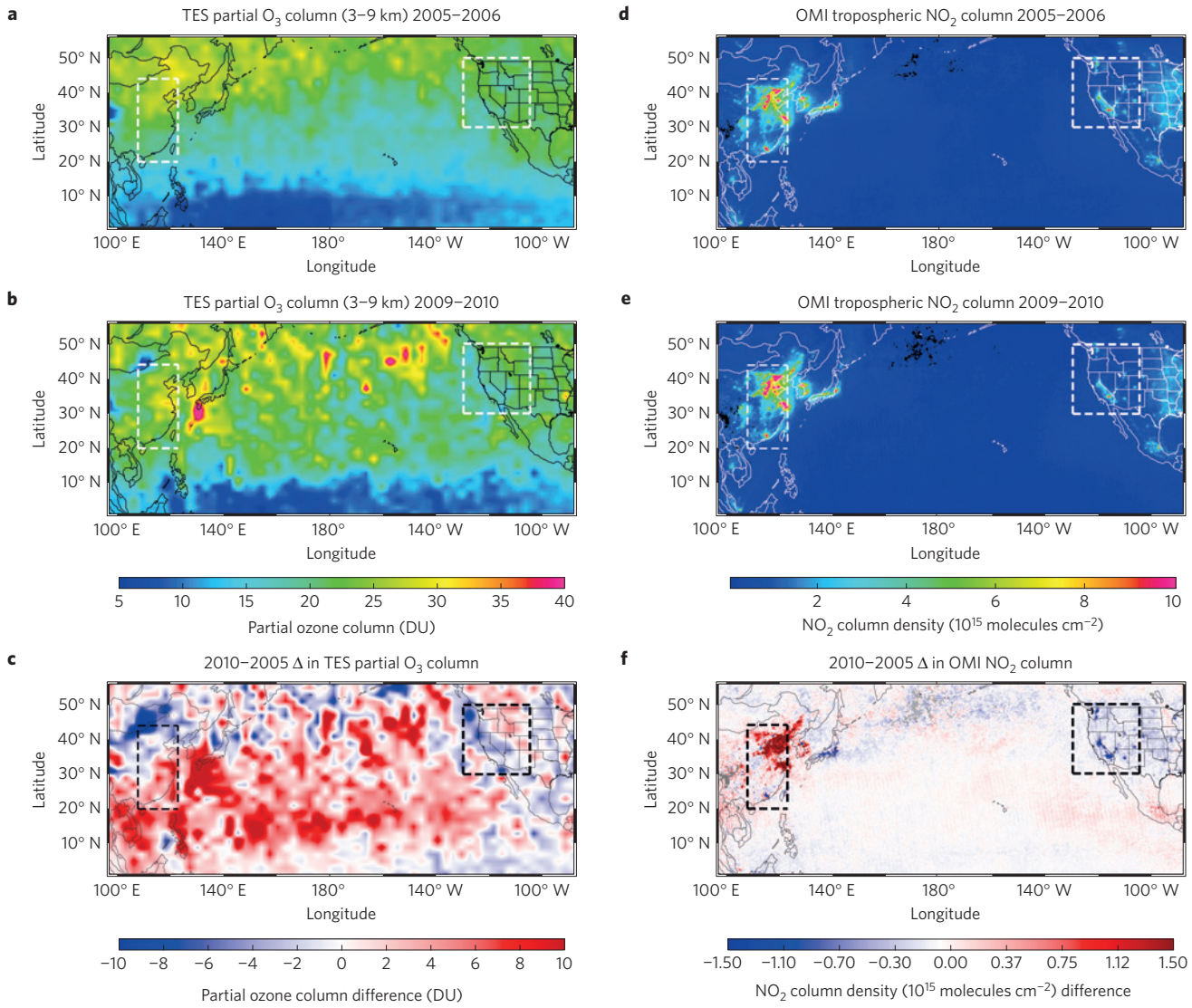

Figure 1 | Summertime tropospheric O_3 and NO_2 distributions for 2005–2006 and 2009–2010 observed by TES and OMI. a, Averaged TES partial O_3 column (3–9 km) for May–August 2005–2006 (clear-sky conditions: cloud top pressure >750 hPa, effective optical depth <50). **b**, Same as **a** but for 2009–2010. **c**, Difference between 2010 and 2005 TES observations. **d**–**f**, Corresponding results from OMI tropospheric NO_2 columns (mostly clear-sky situations: cloud radiance fraction <0.5). TES (OMI) observations have been aggregated over 3° × 2° (0.25° × 0.25°) longitude × latitude grid cells. Dashed lines: Eastern China: 105°–129° E, 18°–42° N and western US: 130°–105° W, 20°–50° N (typically including ~70 TES data points per month).

precursors because both regions are NO_X-limited throughout the photochemically active seasons, and top-down scaling suggests that lower tropospheric O_3 concentrations are 5–15 times less sensitive to changes in anthropogenic volatile organic compounds (VOCs) and CO than to changes in NO_X (ref. 20; Supplementary Information 2). We use TM5 to evaluate the contributions of these different drivers to the observed 2005–2010 O_3 changes (Methods). TM5 with the OMI-based NO_X emissions generally captures the absolute magnitude and temporal evolution of the TES O_3 observations over China (Fig. 2a). Over the western US, TM5 also reproduces the monthly observations, but with slightly larger deviations from TES during the summer months, which we attribute primarily to errors in modelling local influences rather than long-range transport (Supplementary Information 3).

Deseasonalized TES observations (Methods and Fig. 2b,f) show a large, statistically significant ($P = 0.002$, 95% confidence interval, two-tailed) increase in tropospheric O_3 over eastern China of 1.08% yr^{-1} (0.23 DU yr^{-1}) for the period 2005–2010, and a smaller, insignificant increase ($P = 0.16$) over the western US (0.56% yr^{-1}, 0.13 DU yr^{-1}) (Table 1). Local soundings over Beijing[3] show an increase in O_3 of ~5% yr^{-1} (2002–2011) at 3–9 km altitude; co-located TES and TM5 grid cells show an increase of ~3 and ~4% yr^{-1}, respectively.

To investigate the STE contribution to the observed O_3 short-term trends, we examine TM5 simulations with tagged stratospheric O_3 (inflow driven by ECMWF cross-tropopause fluxes of satellite-constrained stratospheric O_3 distributions[22]). These show a substantial positive short-term trend ($P < 0.001$) in the stratospheric contribution, with STE accounting for an increase of ~0.80% yr^{-1} (0.78–0.84) ($P < 0.001$) in the 3–9 km tropospheric O_3 over both regions (Fig. 2c,g, Table 1 and Supplementary Information 4). MLS observations of the Northern Hemisphere mid-latitudes, however, suggest only a small positive trend in the stratospheric contribution to tropospheric O_3 for the period 2005–2010, driven almost entirely by the 2009/2010 El Niño/Easterly shear quasi-biennial oscillation (ref. 16). The large model STE trend seems to arise from an unrealistically large trend in lower stratospheric O_3 as compared to MLS

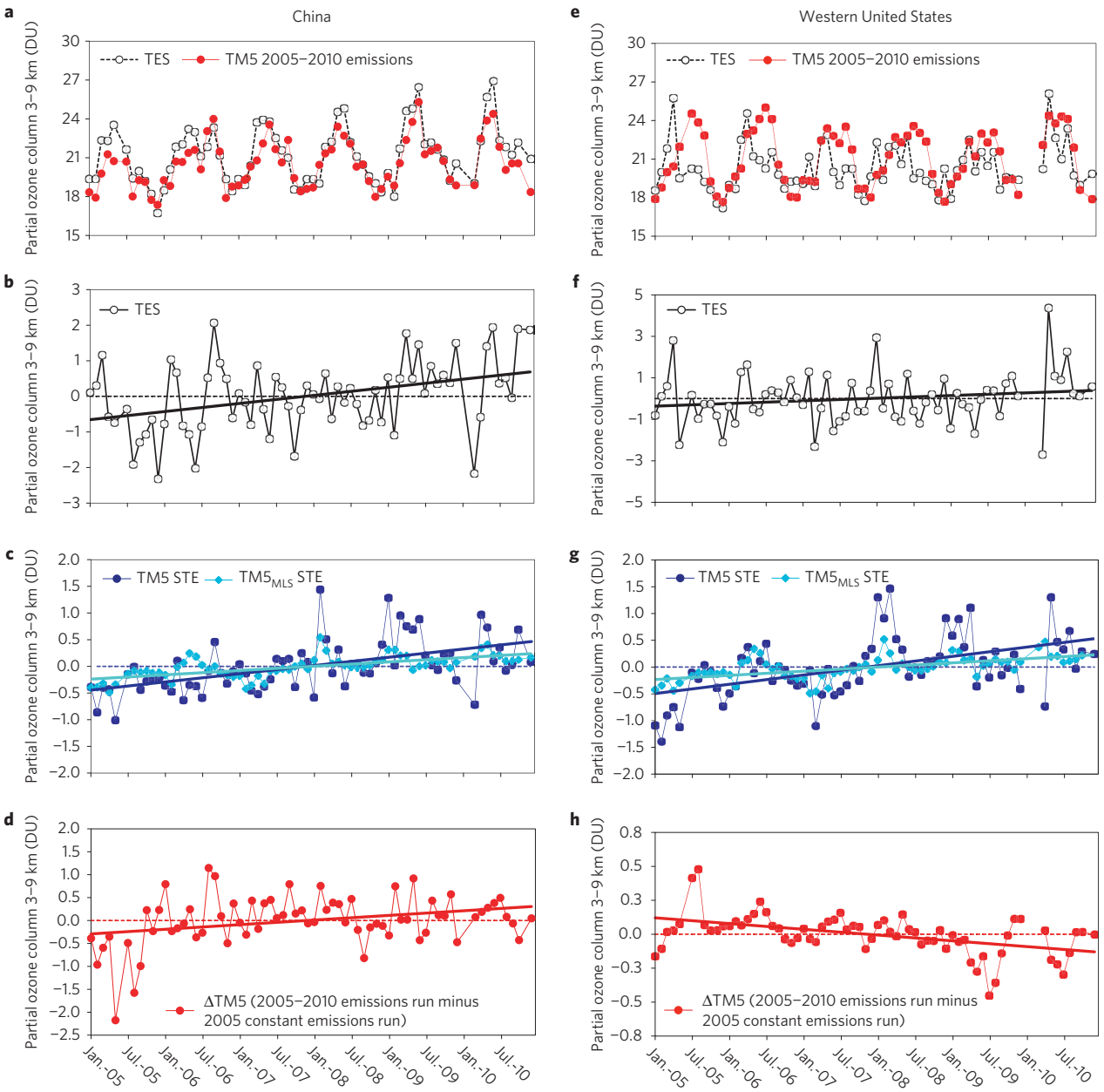

Figure 2 | 2005–2010 observed and simulated changes in monthly tropospheric partial O_3 columns over eastern China and the western US. a–d, Eastern China. **e–h**, Western US. **a**,**e**, TES 3–9 km O_3 time series (dashed black curve) and TM5 simulations (dashed red) with OMI-inferred anthropogenic NO_X emissions. **b–d**,**f–h**, Short-term trends in deseasonalized O_3 columns. **b**,**f**, TES deseasonalized time series (solid black line). **c**,**g**, 2005–2010 changes in the contribution of stratospheric O_3 to the tropospheric column for TM5 (dark blue) and $TM5_{MLS}$ (bright blue). **d**,**h**, Effect of changing NO_X emissions (OMI-inferred 2005–2010 NO_X emissions run minus the constant year 2005 emissions run).

(Supplementary Information 4). To better reflect the considerable uncertainties in STE, we provide a second estimate of the STE contribution to the tropospheric O_3 changes by constraining TM5 lower stratospheric O_3 concentrations using MLS measurements[16] ($TM5_{MLS}$; Supplementary Information 4), which results in a smaller STE contribution of ~0.5% yr^{-1} (Table 1). With the MLS-corrected STE (Fig. 2c,g), the modelled O_3 trend is reduced from 1.33% yr^{-1} to 1.03% yr^{-1} over China and from 0.65% yr^{-1} to 0.27% yr^{-1} over the western US (Table 1). Although $TM5_{MLS}$ trends are slightly lower than those from TM5, both agree with TES trends within their uncertainties.

To quantify the impacts of NO_X emissions changes on the partial O_3 columns, we subtract the TM5 run with updated 2005–2010 NO_X emissions from a simulation with constant 2005 emissions, so that all processes driven by annually varying meteorology, including STE, cancel out. The 21% increase in NO_X emissions between 2005 and 2010 (inferred from monthly OMI observations) is responsible for a 0.10 DU yr^{-1} (0.58% yr^{-1}) trend in tropospheric O_3 over China (Fig. 2d and Table 1). Furthermore, the increases over eastern Asia are strongest in summertime (Supplementary Information 5), indicative of an important role for enhanced photochemical production. For the western US, 21% reductions in OMI-inferred NO_X emissions result in a clearcut decrease (−0.04 DU yr^{-1}) in modelled tropospheric O_3 (Fig. 2h and Table 1). Note that the short-term trends are significantly different from zero despite the relative high standard errors (s.e.m.); the relative changes in the partial O_3 columns for 2005–2010 from TM5 agree well with TES only if the NO_X emissions changes are considered

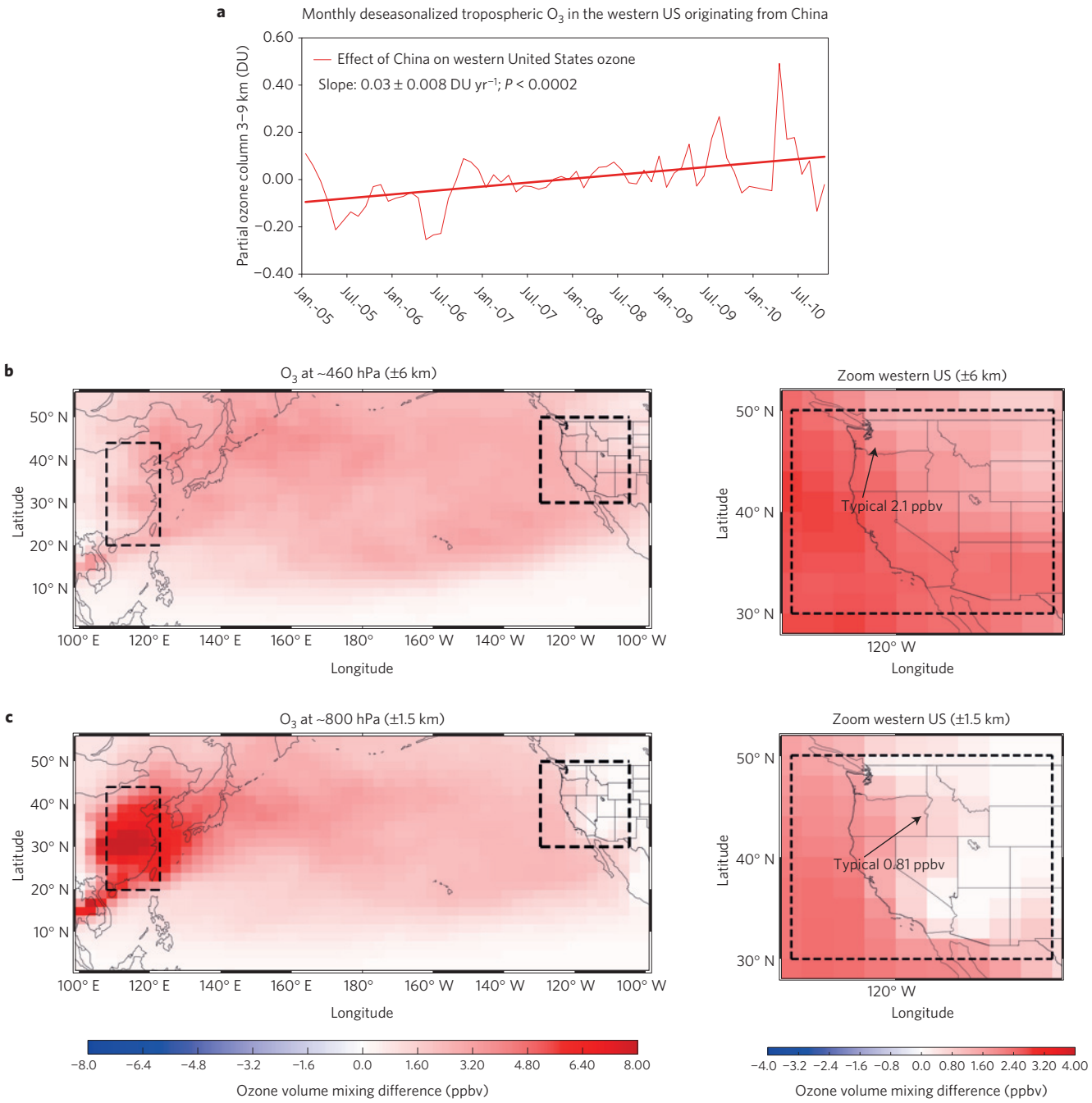

Figure 3 | The effect of Chinese emissions and long-range transport on tropospheric O_3 over the western US. a, Monthly deseasonalized difference between the global TM5 run with observationally constrained 2005–2010 anthropogenic NO_X emissions and the TM5 run with constant 2005 NO_X emissions for China and observationally constrained emissions everywhere else. **b**, Difference in O_3 in the free troposphere (~460 hPa) between the two TM5 runs for April–May 2010 sampled at the Aura overpass time. **c**, As for **b** but showing the lower troposphere (~800 hPa).

(Supplementary Information 2). Over China, the NO_X emissions update results in an increase in O_3 of ~0.6% yr^{-1} and thus explains roughly half of the TM5 short-term trend (1.03–1.33% yr^{-1}, Table 1). Over the western US, non-significant O_3 increases were found ($P = 0.159$ and 0.120 for TES and TM5, respectively), despite the significant NO_X-driven O_3 decrease of 0.2% yr^{-1}.

From the above attribution of O_3 sources, we find that increased STE may have masked out the effects of reductions in anthropogenic NO_X emissions in the US for 2005–2010. A critical question, however, is how the 2005–2010 observed Chinese emissions and O_3 increases have influenced tropospheric O_3 concentrations over the western US (refs 5,23). To obtain a quantitative estimate of the impacts of Chinese emissions alone, we compare the global 2005–2010 emission update simulation against a simulation with constant (year 2005) emissions for China combined with OMI-constrained emissions for the rest of the world (Methods and Supplementary Information 2). In this way, the domestic NO_X emissions reductions in the US and the changes in the other parts of the world are identical in both runs, except for China. The O_3 decrease over the western US associated with both local and Asian NO_X emissions changes is 0.04 DU yr^{-1} (Table 1), but the contribution of emissions and O_3 transport from China to tropospheric O_3 over the western US has grown by 0.03 DU yr^{-1} over 2005–2010 (Fig. 3a). The import from China has thus neutralized

Table 1 | Attribution of absolute and relative changes in 2005–2010 partial O_3 column trends over China and western US.

	China				Western United States			
	Absolute change ±s.e.m. (DU yr^{-1})		Relative change (% yr^{-1})		Absolute change ±s.e.m. (DU yr^{-1})		Relative change (% yr^{-1})	
	TM5	TM5$_{MLS}$	TM5	TM5$_{MLS}$	TM5	TM5$_{MLS}$	TM5	TM5$_{MLS}$
TES observed	0.23 ± 0.07		1.08		0.13 ± 0.09		0.56	
TM5 simulated	0.23 ± 0.07	0.18 ± 0.04	1.33	1.03	0.13 ± 0.16	0.04 ± 0.04	0.65	0.27
STE contribution	0.13 ± 0.03	0.08 ± 0.02	0.78	0.45	0.17 ± 0.04	0.08 ± 0.02	0.84	0.47
NO_X contribution	0.10 ± 0.04		0.58		−0.04 ± 0.01		−0.2	

First row: TES-observed changes in 3–9 km O_3 column (DU yr^{-1} and % yr^{-1}). Second row: Simulated O_3 column changes with OMI-constrained 2005–2010 NO_X emissions for both TM5 and the simulation with MLS-corrected STE (TM5$_{MLS}$). Third row: STE contribution to the simulated O_3 changes for TM5 and TM5$_{MLS}$. Fourth row: O_3 column changes attributable to changing (OMI-inferred) NO_X emissions. Changes are statistically significantly different from zero ($P < 0.05$), except for TES and TM5 trends over western US ($P > 0.15$).

~43% of the 0.07 (= 0.03 + 0.04) DU yr^{-1} O_3 decrease that would have occurred largely in response to air pollution controls in the western US, had Chinese emissions been constant. This is consistent with the spatial pattern of O_3 changes seen in Fig. 1c. O_3 over the western US decreased only in regions with very large NO_X reductions; NO_X reductions elsewhere (Fig. 1f) have been offset by a combination of STE and Chinese emissions.

The influence of Chinese pollution on the western US is largest during spring[5], with 2010 (Fig. 3b,c) representing the maximum Chinese influence for the time series (Fig. 3a). The contribution to western US free-tropospheric O_3 is widespread (Fig. 3b) and larger than the contribution to near-surface O_3 (Fig. 3c). Our estimate of the western US response to Chinese emission changes is of the same order of magnitude as reported values for source–receptor relationships established from other models[6,11,24], which have shown the importance of large-scale transport patterns and processes such as sustained O_3 production during trans-Pacific transport driven by decomposition of nitrogen reservoirs in descending air masses[12,25] in generating this response. The 2010 peak is probably related to the strong El Niño[16], which favoured efficient transport towards the West Coast[7,15].

The rapid increase in tropospheric O_3 (almost 7% over six years) from 2005 to 2010 detected by TES over China is evocative of much stronger changes in the lower troposphere (Fig. 3c). TM5 simulations reproduce the observed O_3 increases within their uncertainties (Supplementary Information 6 and Supplementary Table 2) when changes in NO_X emissions and STE are considered. Our results indicate that policy-driven domestic emissions reductions decrease free-tropospheric O_3 over the western US, but the effect is offset by changes in STE combined with increasing long-range inflow of O_3 and its precursors from China. This Chinese export offsets ~43% of a nominal 0.07 DU yr^{-1} domestic O_3 reduction, suggesting that air quality and regional climate change mitigation policies could eventually have limited impact if not considered in a global context, at least for free-tropospheric O_3 and its precursors[10].

Methods

Methods and any associated references are available in the online version of the paper.

Received 9 April 2015; accepted 26 June 2015;
published online 10 August 2015

References

1. van der A, R. J. *et al.* Trends, seasonal variability and dominant NO_x source derived from a ten year record of NO_2 measured from space. *J. Geophys. Res.* **113,** D04302 (2008).
2. Tanimoto, H. Increase in springtime tropospheric ozone at a mountainous site in Japan for the period 1998–2006. *Atmos. Environ.* **43,** 1358–1363 (2009).
3. Wang, Y. *et al.* Tropospheric ozone trend over Beijing from 2002–2010: Ozonesonde measurements and modeling analysis. *Atmos. Chem. Phys.* **12,** 8389–8399 (2012).
4. Parrish, D. D., Millet, D. B. & Goldstein, A. H. Increasing ozone in marine boundary layer inflow at the west coasts of North America and Europe. *Atmos. Chem. Phys.* **9,** 1303–1323 (2009).
5. Cooper, O. R. *et al.* Increasing springtime ozone mixing ratios in the free troposphere over western North America. *Nature* **463,** 344–348 (2010).
6. Brown-Steiner, B. & Hess, P. Asian influence on surface ozone in the United States: A comparison of chemistry, seasonality, and transport mechanisms. *J. Geophys. Res.* **116,** D17309 (2011).
7. Lin, M. *et al.* Transport of Asian ozone pollution into surface air over the western United States in spring. *J. Geophys. Res.* **117,** D00V07 (2012).
8. IPCC *Climate Change 2007: The Physical Science Basis* (eds Solomon, S. *et al.*) (Cambridge Univ. Press, 2007).
9. Arneth, A. *et al.* Terrestrial biogeochemical feedbacks in the climate system. *Nature* **3,** 525–532 (2010).
10. Bowman, K. & Henze, D. K. Attribution of direct ozone radiative forcings to spatially resolved emissions. *Geophys. Res. Lett.* **39,** L22704 (2012).
11. Dentener, F., Keating, T. & Akimoto, H. *Air Pollution Studies No. 17* (United Nations, 2010).
12. Zhang, L. *et al.* Transpacific transport of ozone pollution and the effect of recent Asian emission increases on air quality in North America: An integrated analysis using satellite, aircraft, ozonesonde, and surface observations. *Atmos. Chem. Phys.* **8,** 6117–6136 (2008).
13. Fiore, A. M. *et al.* Multimodel estimates of intercontinental source-receptor relationships for ozone pollution. *J. Geophys. Res.* **114,** D04301 (2009).
14. Hess, P. & Zbinden, R. Stratospheric impact on tropospheric ozone variability and trends: 1990–2009. *Atmos. Chem. Phys.* **13,** 649–674 (2013).
15. Lin, M., Horowitz, L. W., Oltmans, S. J., Fiore, A. M. & Fan, S. Tropospheric ozone trends at Mauna Loa Observatory tied to decadal climate variability. *Nature Geosci.* **7,** 136–143 (2014).
16. Neu, J. L. *et al.* Tropospheric ozone variations governed by changes in the stratospheric circulation. *Nature Geosci.* **7,** 340–344 (2014).
17. Oltmans, S. J. *et al.* Recent tropospheric ozone changes—A pattern dominated by slow or no growth. *Atmos. Environ.* **67,** 331–351 (2013).
18. Parrish, D. D. *et al.* Long-term changes in lower tropospheric baseline ozone concentrations: Comparing chemistry-climate models and observations at northern midlatitudes. *J. Geophys. Res.* **119,** 5719–5736 (2014).
19. Huijnen, V. *et al.* The global chemistry transport model TM5: Description and evaluation of the tropospheric chemistry version 3.0. *Geosci. Mod. Develop.* **3,** 445–473 (2010).
20. Lamsal, L. N. *et al.* Application of satellite observations for timely updates to global anthropogenic NO_x emission inventories. *Geophys. Res. Lett.* **38,** L05810 (2011).
21. Russell, A. R., Valin, L. C. & Cohen, R. C. Trends in OMI NO_2 observations over the United States: Effects of emission control technology and the economic recession. *Atmos. Chem. Phys.* **12,** 12197–12209 (2012).
22. van der A, R. J., Allaart, M. A. F. & Eskes, H. J. Multi sensor reanalysis of total ozone. *Atmos. Chem. Phys.* **10,** 11277–11294 (2010).
23. Cooper, O. R. *et al.* Long-term ozone trends at rural ozone monitoring sites across the United States, 1990–2010. *J. Geophys. Res.* **117,** D22307 (2012).
24. Sudo, K. & Akimoto, H. Global source attribution of tropospheric ozone: Long-range transport from various source regions. *J. Geophys. Res.* **112,** D12302 (2007).
25. Jaffe, D., Mckendry, I., Anderson, T. & Price, H. Six 'new' episodes of trans-Pacific transport of air pollutants. *Atmos. Environ.* **37,** 391–404 (2003).

Acknowledgements

This research was funded by the Netherlands Organization for Scientific Research, NWO Vidi grant 864.09.001. We acknowledge the free use of tropospheric NO_2 columns from the OMI sensor from www.temis.nl. Part of this research was carried out at the Jet Propulsion Laboratory, California Institute of Technology, under a contract with the National Aeronautics and Space Administration. A grant from NASA ROSES NNH10ZDA001N-AURA and from the European Community's Seventh Framework Programme under grant agreement no 607405 (QA4ECV) supported part of this research.

Author contributions

W.W.V. performed the research, drafted the manuscript, prepared the figures and developed the analysis methods. J.L.N. provided analysis and interpretation of the MLS O_3 measurements and aided in drafting the manuscript. J.E.W. contributed to the development of TM5 and the nested anthropogenic emission estimates, and supported the data interpretation. K.W.B. and J.R.W. provided analysis tools and interpretation. K.W.B., J.L.N. and J.R.W. are responsible for the TES experiment and instrument and project planning. K.F.B. is responsible for the Dutch OMI NO_2 data product, aided in drafting the manuscript and methods, and supported the development of the analysis methods and interpretation. All authors contributed to discussions of the results and preparation of the manuscript.

Additional information

Supplementary information is available in the online version of the paper. Reprints and permissions information is available online at www.nature.com/reprints. Correspondence and requests for materials should be addressed to W.W.V.

Competing financial interests

The authors declare no competing financial interests.

Methods

TES tropospheric O_3 data. TES global survey standard products consist of 16 orbits of nadir vertical profiles with 5×8 km^2 horizontal resolution spaced 1.6° along the polar Sun-synchronous orbit track. In general, the TES vertical resolution for O_3 profiles is 6–7 km, corresponding to ~1–2 degrees of freedom (DOF) in the troposphere. Nonlinear spectral fitting of retrieval parameters is applied based on the optimal estimation technique for deriving TES O_3 from radiative transfer forward model simulations and observed radiances. A priori O_3 information is taken from monthly mean simulations from the MOZART model and averaged over $10° \times 60°$ grids (latitude by longitude), and the averaging kernel (AK) is used to evaluate the vertical sensitivity of TES-retrieved O_3. We have used V004 data (2005–2009) and V005 data (2010). Validation of these data has demonstrated that TES accurately captures spatial and temporal patterns in O_3 and, critical to this study, does not exhibit a trend in the retrieval bias[26]. References for TES O_3 retrievals and validation can be found in ref. 26. TES measurements continue, but have limited availability after 2010.

OMI tropospheric NO_2 column data. OMI tropospheric NO_2 columns are retrieved under cloud-free conditions (cloud fraction below 20%) at ~13 h 30 h local time (DOMINO v2; ref. 27) with a three-step approach: retrieval of NO_2 slant columns with Differential Optical Absorption Spectroscopy (405–465 nm wavelength range, spectral resolution of 0.5 nm), followed by assimilation of OMI NO_2 slant columns in the global chemistry–transport model TM4 for providing stratospheric background and a priori NO_2 profile shapes needed to calculate the tropospheric air mass factors. These are then used to convert the tropospheric slant columns into vertical columns. The OMI pixel size varies from 24 km × 13 km at nadir to 140 km × 26 km at the edges of the swath. Individual pixels were re-gridded to 2° latitude by 3° longitude, consistent with the TM5 grid. Pixels affected by the OMI row anomaly were excluded for the entire 2005–2010 period[27]. OMI tropospheric NO_2 vertical column densities show substantial sensitivity to boundary layer NO_2 levels and the DOMINO v2 product has been used and validated extensively[28].

MLS stratospheric O_3 data. MLS measures microwave thermal emissions by scanning the Earth's atmospheric limb. The measurements have a horizontal resolution of ~200–500 km and are spaced ~165 km apart along-track, for a total of ~3,500 high-resolution (~2–3 km) vertical O_3 profiles and other species globally each day. Like TES, MLS retrievals are based on the optimal estimation technique. The single-profile precision for the 215–100 hPa O_3 measurements used here is ~0.04 ppmv, and biases against ozonesonde measurements are <20% (ref. 29). We show results for v2.2 MLS O_3 measurements, but find similar results with v3.3.

TM5 (Tracer Model 5) chemistry–transport model. TM5 (ref. 19) v3 simulates tracers at 34 vertical layers (surface-0.1 hPa) in a standard $3° \times 2°$ (longitude/latitude) horizontal resolution using ERA-interim reanalysis meteorological fields. The chemistry scheme in TM5 is based on the Carbon-Bond Mechanism IV (CBM-IV). Stratospheric O_3 is constrained by assimilated total O_3 columns from a multi-sensor reanalysis data set[22]. The anthropogenic emission inventories were taken from the RETRO project, supplemented with those from the REAS (ref. 30) inventory for the Asian region. Biogenic emissions were adopted from climatologic values, either from GEIA (1990) or from the 12-year (1983–1995) average output of the ORCHIDEE model. Biomass burning emissions originated from the Global Fire Emissions Database version 2 (GFEDv2) 8-day inventories and lightning NO_X emissions were parameterized. We have run the TM5 model for the period 2005–2010 with a spin-up period of one year (2004) using the relevant meteorology and available emission inventories.

Top-down NO_X emissions estimated from OMI NO_2. We extend the mass balance approach[20] to estimate top-down anthropogenic NO_X emissions globally based on OMI NO_2 observations from 2005 to 2010. Surface NO_X emissions are strongly related to satellite observations of tropospheric NO_2 columns owing to the short NO_X lifetime combined with the high NO_2/NO_X ratio in the boundary layer. We first established the relationship between changes in surface NO_X emissions and changes in tropospheric NO_2 columns in TM5 by computing the sensitivity of modelled tropospheric NO_2 columns to increases in surface NO_X emissions. We then apply equation (1), effectively scaling the a priori emissions (from RETRO (ref. 31) supplemented with REAS (ref. 30) for the Asian region) with the relative trends observed by OMI, taking into account the response of NO_2 columns to changing NO_X emissions (so-called β-factor). We further use a monthly scaling factor γ ($\gamma = N_{t,OMI}/N_{t,TM5}$, where $N_{t,OMI}$ is the OMI NO_2 value for a specific month of year t and $N_{t,TM5}$ is the TM5 NO_2 value for the same month and year) to match the TM5 tropospheric NO_2 columns to OMI observations. This also provides better agreement with anthropogenic NO_X emissions reported in the literature[32,33] (discussed below) than straightforward application of the approach in ref. 20. The monthly time-dependent top-down NO_X emissions (E_t) are calculated as:

$$E_t = E_a \left(1 + \beta \frac{N_{t,OMI} - N_{a,OMI}}{N_{a,OMI}}\right) \gamma \quad (1)$$

where E_a represents the a priori NO_X emissions (subscript a refers to a priori) in TM5 (from the 2005 nested RETRO/REAS inventories), β is the sensitivity, which relates an increase of 15% in surface emissions of NO_X in TM5 to resulting changes in modelled tropospheric NO_2, $N_{a,OMI}$ is the OMI NO_2 for a specific month of 2005. We compute β on a monthly basis using the TM5 simulation for 2006. NO_X emissions in TM5 are distributed over the days of the month and over the hours of the day following prescribed day-of-week and hour-of-day patterns. The monthly values are then used to calculate the top-down estimates (E_t) for each month of year t. Absolute uncertainties in E_t are considerable (order 50%) because of errors in both TM5 and the OMI retrievals, but the top-down estimates capture the changes in NO_X emissions associated with relevant variations in economic activity and environmental legislation in different parts of the world between 2005 and 2010. At the grid cell size of TM5, the β-factors describing the sensitivity of NO_2 columns to NO_X emissions are largely driven by the seasonal cycle in photochemistry, suggesting a small role for nonlinear chemistry in modelling and explaining O_3 changes over time. The time series of tropospheric NO_2 columns observed by OMI over China and the western US used for updating the NO_X emissions in TM5 are shown in Supplementary Fig. 1 (more details in Supplementary Information 2). The yearly OMI-inferred NO_X emissions for China and the western US are given in Supplementary Table 1 (see Supplementary Information 2). We find a 21% increase in NO_X emissions over China and a 21% reduction over the western US, comparable to reported estimates[32] for 2005–2010 (27% growth in Chinese NO_X emissions and 23% decrease over the United States) and estimates[20] based on SCIAMACHY (2006–2009 increase in anthropogenic emissions of 19% over East Asia and decrease of 6% over North America), given differences in time period and area. The anthropogenic NO_X emissions and their evolution are of the same order of magnitude as in ref. 33 for the given regions.

Comparing TES tropospheric O_3 with TM5. For comparisons with TES, the TM5 O_3 profiles from simulations with constant 2005 emissions and with 2005–2010 updated emissions were sampled along the AURA orbit track at the observation times and interpolated onto the TES pressure grid. Using partial column averages, no substantial difference is observed, whether or not the vertical sensitivity of each TES retrieval[26] is considered.

TM5 simulations. Attribution of the observed tropospheric O_3 values to various sources is based on three different TM5 model runs. A first (base) run for the period 2005–2010 consists of TM5 simulations using a fixed anthropogenic emission scenario based on 2005 values of the REAS inventory, resulting in tropospheric O_3 changes due to meteorology, long-range O_3 transport and STE. The second run evaluates the effect of changing anthropogenic NO_X emissions on tropospheric O_3 by updating the emissions based on OMI NO_2 observations for the entire 2005–2010 period. By comparing the first and second runs the effect of the changes in NO_X emissions on O_3 production can be assessed because the changes due to STE and meteorology cancel out. Tagged O_3 (O_{3s}) TM5 simulations allow us to quantify the contribution of STE, tracing the O_3 originating from the stratosphere to the troposphere, where it is subject to loss processes. A final run was set up to evaluate the influence of increased NO_X emissions and O_3 production in China on the United States by using the OMI-based update of anthropogenic emissions worldwide, except for China, where year 2005 NO_X emissions were used. Subtracting this run from the world-wide updated second run allows us to isolate the effect of growing Chinese emissions on the United States with respect to O_3 pollution.

Time series analysis. Deseasonalized monthly time series (both from satellite data and model output) are computed by subtracting from each monthly value the six-year average for that specific month.

MLS-corrected TM5 stratosphere–troposphere O_3 exchange. We constrain TM5 STE in a two-step linear regression (see also Supplementary Information 4). First we establish a relationship between the model's lower stratospheric O_3 (at 200–250 hPa) and the monthly averaged contribution of TM5 STE O_3 to the 3–9 km partial column for 30–50° N (see Supplementary Fig. 5). We calculate a corrected zonal mean STE contribution using 215 hPa MLS O_3 measurements for this same latitude band. We then diagnose the relationship between TM5 STE over China and the Western US and the zonal mean TM5 STE to derive corrected regional STE trends. Giving 50% weight to MLS retrievals, we calculate a lower but still positive contribution of STE to the TM5 short-term O_3 for both China and the western US, as reported in Table 1.

Data sources. All Aura satellite measurements are publicly available. TES O_3 data are available at http://tes.jpl.nasa.gov; OMI NO_2 data are available at http://www.temis.nl/airpollution/no2.html; MLS O_3 data are available at https://mls.jpl.nasa.gov.

Code availability. The TM5 model code used to generate the simulations analysed here is available at http://tm5.sourceforge.net.

References

26. Verstraeten, W. W. *et al.* Validation of six years of TES tropospheric ozone retrievals with ozonesonde measurements: Implications for spatial patterns and temporal stability in the bias. *Atmos. Meas. Tech.* **6,** 1413–1423 (2013).
27. Boersma, K. F. *et al.* An improved tropospheric NO_2 column retrieval algorithm for the Ozone Monitoring Instrument. *Atmos. Meas. Tech.* **4,** 1905–1928 (2011).
28. Irie, H. *et al.* Quantitative bias estimates for tropospheric NO_2 columns retrieved from SCIAMACHY, OMI, and GOME-2 using a common standard for East Asia. *Atmos. Meas. Tech.* **5,** 2403–2411 (2012).
29. Livesey, N. J. *et al.* Validation of Aura Microwave Limb Sounder O_3 and CO observations in the upper troposphere and lower stratosphere. *J. Geophys. Res.* **113,** D15S02 (2008).
30. Ohara, T. *et al.* An Asian emission inventory of anthropogenic emission sources for the period 1980–2020. *Atmos. Chem. Phys.* **7,** 4419–4444 (2007).
31. Schultz, M. G. *et al. REanalysis of the TROpospheric Chemical Composition Over the Past 40 Years* (*RETRO*)*—A Long-Term Global Modeling Study of Tropospheric Chemistry* Report no. 48/2007, 30 (Max Planck Institute for Meteorology, 2007).
32. Streets, D. G. *et al.* Emissions estimation from satellite retrievals: A review of current capability. *Atmos. Environ.* **77,** 1011–1042 (2013).
33. Granier, C. *et al.* Evolution of anthropogenic and biomass burning emissions of air pollutants at global and regional scales during the 1980–2010 period. *Clim. Change* **109,** 63–190 (2011).